Soft Matter

PAPER

View Article Online
View Journal

Cite this: DOI: 10.1039/c6sm02230h

Gaussian fluctuations of spatially inhomogeneous polymers†

Yohai Bar-Sinai*‡ and Eran Bouchbinder

Inhomogeneous polymers, such as partially cofilin-bound actin filaments, play an important role in various natural and biotechnological systems. At finite temperatures, inhomogeneous polymers exhibit non-trivial thermal fluctuations. More broadly, these are relatively simple examples of fluctuations in spatially inhomogeneous systems, which are less understood compared to their homogeneous counterparts. Here we develop a statistical theory of torsional, extensional and bending Gaussian fluctuations of inhomogeneous polymers (chains), where the inhomogeneity is an inclusion of variable size and stiffness, using both continuum and discrete approaches. First, we analytically calculate the complete eigenvalue and eigenmode spectra within a continuum field theory. In particular, we show that the wavenumber inside and outside of the inclusion is nearly linear in the eigenvalue index, with a nontrivial coefficient. Second, we solve the corresponding discrete problem and highlight fundamental differences between the continuum and discrete spectra. In particular, we demonstrate that above a certain wavenumber the discrete spectrum changes qualitatively and discrete evanescent eigenmodes, which do not have continuum counterparts, emerge. The implications of these differences are explored by calculating fluctuation-induced forces associated with free-energy variations with either the inclusion properties (*e.g.* inhomogeneity formed by adsorbing molecules) or with an external geometric constraint. The former, which is the fluctuation-induced contribution to the adsorbing molecule binding force, is shown to be affected by short wavelengths and thus cannot be calculated using the continuum approach. The latter, on the other hand, is shown to be dominated by long wavelength shape fluctuations and hence is properly described by the continuum theory.

Received 30th September 2016,
Accepted 8th December 2016

DOI: 10.1039/c6sm02230h

www.rsc.org/softmatter

1 Introduction

Spatially inhomogeneous systems are ubiquitous in the natural and manmade world around us, giving rise to intriguing physical behaviors as compared to their homogeneous counterparts. For example, glassy systems – which feature inhomogeneity/disorder on small lengthscales – still pose great challenges in condensed-matter and statistical physics.[1–3] Low-dimensional systems, such as rods, beams and polymers, also feature interesting behaviors in the presence of spatial inhomogeneities in their properties. When these systems are excited externally, either by mechanical perturbations or by coupling to a heat bath, they exhibit non-trivial responses and fluctuations associated with the spatial inhomogeneity. Thermal and entropic effects are known to play a major role in a broad range of soft matter and biophysics problems where polymers and biopolymers are considered.[4,5] Therefore, it is important to understand the effect of spatial inhomogeneity on the fluctuations of polymers.[6–8]

To address this problem we study in this paper the mechanics and statistical thermodynamics of spatially inhomogeneous one-dimensional polymers where the inhomogeneity takes the form of an inclusion of finite length which is mechanically softer than the rest of the polymer. The polymer is assumed to be submerged in a solvent of a fixed temperature such that it undergoes overdamped equilibrium thermal fluctuations under certain constraints. There are many physical systems that might give rise to such a situation. For example, actin filaments in cells are known to significantly soften in regions where cofilin molecules bind to them,[9–12] so partially cofilin-decorated actin filaments are spatially inhomogeneous. Other natural and man-made systems can exhibit similar spatial inhomogeneity.[6,13–16]

Our discussion, while being motivated by these realistic and important examples, remains rather general and independent of the particular details of the underlying physical system. This is achieved by considering general Hamiltonians in the small gradient approximation, *i.e.* generic quadratic Hamiltonians (energy functionals).

Chemical Physics Department, Weizmann Institute of Science, Rehovot 7610001, Israel. E-mail: eran.bouchbinder@weizmann.ac.il

† Electronic supplementary information (ESI) available. See DOI: 10.1039/c6sm02230h

‡ Current address: Harvard University, School of Engineering and Applied Sciences, 29 Oxford St., Cambridge 02138, Massachusetts, USA. E-mail: ybarsinai@gmail.com

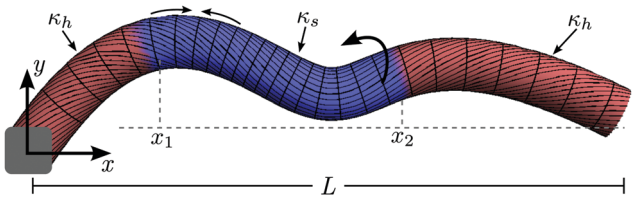

Fig. 1 Schematic sketch of a fluctuating polymer, showing bending, extensional and twisting motions. The polymer length L is assumed to be of the order of the persistence length (for bending) such that the fluctuations can be treated to linear order as deviations from a straight line. The purple segment represents a region with a reduced elastic modulus. The gray square at the origin represents pinning of the polymer at one end, the other end being free.

The geometry of the fluctuating polymer is sketched in Fig. 1. The polymer's length is assumed to be comparable to the bending persistence length such that dynamics can be approximately described in terms of Cartesian coordinates and do not necessitate arc-length parametrization. In the context of torsional fluctuations of the polymer, the energy functional is quadratic in the gradient of the twist angle, while in the context of extensional fluctuations of the polymer the energy functional is quadratic in the gradient of the longitudinal displacement along the polymer. These fluctuations are represented by the thin curved longitudinal lines in Fig. 1 (torsion) and by the uneven spacing of circumferential lines (extension). The resulting energy functional is the same in these two cases.

In the context of bending fluctuations of the polymer, the energy functional is quadratic in the local curvature, which in itself is a second derivative of the out-of-plane deflection of the polymer in the small gradient approximation, *cf.* Fig. 1. This is nothing but the classical one-dimensional Helfrich Hamiltonian in the absence of surface tension.[5,17] As such, from a more theoretical perspective, we consider the classical example of massless§ quadratic field theory in one spatial dimension with position-dependent properties, applicable to a broad range of other physical systems.[18]

Gaussian fluctuations of such one-dimensional fields, *i.e.* when the quadratic approximation is adopted, are oftentimes addressed in the framework of statistical field theory. In this framework a continuum approach is invoked and macroscopic variables of interest are assumed to vary slowly in space. One of our goals here is to understand to what extent the problem can be described by the continuum approach and when does it break down. To that aim, we solve the problem using both a continuum field theory and its discrete counterpart.

We highlight the fundamental differences between the continuum and discrete spectra of eigenvalues and eigenmodes, and explore the implications of these differences in relation to two physically realistic fluctuation-induced forces. The first one is a fluctuation-induced force associated with free-energy variations with respect to the properties of the inclusion (*e.g.* formed by adsorbing molecules, in which case it is the fluctuation-induced contribution to the binding force of the adsorbing molecules), while the second is a fluctuation-induced force associated with free-energy variations with respect to an external geometric constraint (*e.g.* a confining wall). We show that while the continuum theory is valid in the latter case, it breaks down in the former.

§ In the jargon of statistical field theory, "massless" refers to the lack of a term proportional to w^2, which in our case would correspond to an external potential. Here, we also work in the overdamped limit, which in this context might be termed "inertialess".

2 Mathematical formulation

We consider a spatially inhomogeneous one-dimensional polymer of length L, consisting of N monomeric units, submerged in a solvent of temperature T. $x \in [0,L]$ is the coordinate along the polymer. The inhomogeneous polymer is treated at the continuum level as a one-dimensional beam/rod characterized by position-dependent mechanical properties along its axis x. The polymer's length is assumed to be comparable to its persistence length with respect to torsional, extensional and bending fluctuations, which implies that the polymer is semi-flexible and hence is fully characterized by its elastic energies.

For concreteness, we consider a polymer composed of 3 locally homogeneous regions with sharp interfaces between them, *cf.* Fig. 1. In other words, we consider an inclusion inside a polymer such that the space-dependent elastic modulus reads

$$\kappa(x) = \begin{cases} \kappa_s & x_1 < x < x_2 \\ \kappa_h & x < x_1 \text{ or } x > x_2 \end{cases}. \quad (1)$$

where κ equals κ_s inside the inclusion and κ_h otherwise. The subscripts h and s denote "hard" and "soft", respectively, so $\kappa_h > \kappa_s$. Here, κ refers generically to either of the torsional, extensional or bending moduli.

We consider the small gradient approximation in which torsional, extensional and bending are described by quadratic energy functionals. At the continuum level, this leads to Gaussian fluctuations that are controlled by either of the two quadratic energy functionals:

$$U^{(1)}(x,t) = \frac{1}{2}\int_0^L \kappa(x)\left(\frac{\partial w(x,t)}{\partial x}\right)^2 \mathrm{d}x,$$
$$U^{(2)}(x,t) = \frac{1}{2}\int_0^L \kappa(x)\left(\frac{\partial^2 w(x,t)}{\partial x^2}\right)^2 \mathrm{d}x, \quad (2)$$

where $w(x,t)$ is a fluctuating field and $\kappa(x)$ is its related modulus. Torsional and extensional fluctuations are described by the former, while bending fluctuations are described by the latter. A sketch of the geometry is given in Fig. 1, which shows all three types of motions. In torsional dynamics $w(x)$ represents the twist angle, measured relative to an *a priori* given equilibrium twist angle profile $\theta_0(x)$.[19] In extensional dynamics, $w(x)$ measures the longitudinal displacement along the axis of the polymer. In bending dynamics, $w(x)$ measures the normal deviation of the polymer from a straight line, *i.e.* the out-of-plane deflection (we assume that the polymer does not feature any intrinsic curvature). In the case of a homogeneous polymer,

i.e. constant κ, $U^{(2)}$ reduces to the standard worm-like-chain model (in the limit of short L).

The very same problem can be formulated at the discrete level, making reference to monomeric degrees of freedom and lengthscales. In particular, the discrete analogs of eqn (2) take the form

$$\begin{aligned} U^{(1)} &= \frac{1}{2}\sum_i \kappa_i \left(\frac{w_i - w_{i-1}}{a}\right)^2 a, \\ U^{(2)} &= \frac{1}{2}\sum_i \kappa_i \left(\frac{w_{i+1} + w_{i-1} - 2w_i}{a^2}\right)^2 a, \end{aligned} \tag{3}$$

where $a \equiv L/N$ is a monomeric lengthscale, κ_i and w_i are the discrete versions of $\kappa(x)$ and $w(x)$, respectively, and i is the monomer index.

Eqn (2) and (3) are representative of a wide class of physical systems whose energy functionals, in the quadratic approximation, can be written as

$$\begin{aligned} U &= \frac{1}{2}\langle w(x)|\mathfrak{L}|w(x)\rangle = \frac{1}{2L}\int_0^L w(x)\mathfrak{L}\{w(x)\}\mathrm{d}x, \\ U &= \frac{1}{2}\langle \boldsymbol{w}|\boldsymbol{H}|\boldsymbol{w}\rangle = \frac{1}{2}\sum_{i,j} w_i H_{ij} w_j, \end{aligned} \tag{4}$$

where $\boldsymbol{H}$ is a real symmetric positive definite matrix and $\mathfrak{L}$ is a self-adjoint real differential operator.[20] Eqn (2) and (3) are recovered from eqn (4) with the proper identification of the dynamical operator. For the discrete theory, one clearly has $\boldsymbol{H} = \boldsymbol{\nabla}\boldsymbol{\nabla}U$. For the continuum theory, one finds that the dynamical operators related to $U^{(1)}$ and $U^{(2)}$ are, respectively,

$$\begin{aligned} \mathfrak{L}^{(1)}\{w\} &= -L\frac{\partial}{\partial x}\left(\kappa(x)\frac{\partial w}{\partial x}\right) \quad \text{for } U^{(1)}, \\ \mathfrak{L}^{(2)}\{w\} &= -L\frac{\partial^2}{\partial x^2}\left(\kappa(x)\frac{\partial^2 w}{\partial x^2}\right) \quad \text{for } U^{(2)}. \end{aligned} \tag{5}$$

We adopt here the convention that the eigenvalues of $\mathfrak{L}$ or $\boldsymbol{H}$ are of energy dimensions, and accordingly the variables w_i and $w(x)$ are dimensionless. In addition, it would be useful to introduce the dimensionless parameters ϕ and Δ:

$$\phi \equiv \frac{x_2 - x_1}{L}, \tag{6}$$

$$\Delta \equiv \left(\frac{\kappa_\mathrm{h}}{\kappa_\mathrm{s}}\right)^{1/2} \quad \text{for} \quad U^{(1)}, \quad \Delta \equiv \left(\frac{\kappa_\mathrm{h}}{\kappa_\mathrm{s}}\right)^{1/4} \quad \text{for} \quad U^{(2)},$$

which are measures of the inclusion size and contrast, respectively. Note that $0 \leq \phi \leq 1$ and $\Delta \geq 1$. Finally, in order to completely define the problem one needs to specify also the external boundary conditions at $x = 0,L$. Here we take the polymer to be fixed (pinned) at $x = 0$ and free at $x = L$. Mathematically, this means

$$w(0) = w'(L) = 0 \quad \text{for} \quad U^{(1)}, \tag{7}$$

$$w(0) = w'(0) = w''(L) = w'''(L) = 0 \quad \text{for} \quad U^{(2)},$$

where a prime denotes partial differentiation with respect to x. For the discrete formulation, this amounts to setting $w_i = 0$ for $i < 1$ and $\kappa_i = 0$ for $i > N$. Choosing different boundary conditions does not qualitatively change the results presented below.

3 Eigenmode analysis: continuum theory

Gaussian fluctuations are fully determined by the eigenvalues of the relevant dynamical operator. Consequently, an essential step in the statistical thermodynamic calculations to follow is finding the eigenvalues and the corresponding eigenmodes of $\mathfrak{L}$ or $\boldsymbol{H}$. This will be the subject of this section and the next one. In this section we calculate the eigenmodes within the continuum theory, and show that the wavenumbers have a constant density. In Section 4 the corresponding discrete problem is solved and the differences between the results are discussed.

3.1 General form of the eigenmodes

The calculation of the eigenmodes is very much in the spirit of standard wave theory analysis of reflection and refraction from a sharp material boundary, or of the quantum mechanical treatment of transmission over a potential barrier step. The eigenmodes w_q are functions that satisfy the continuum eigenvalue equation – the Sturm–Liouville problem:

$$\mathfrak{L}w_q(x) = \lambda_q w_q(x), \tag{8}$$

where λ_q is the eigenvalue associated with w_q. Solving eqn (8) is in general a non-trivial task. However, since $\kappa(x)$ is locally constant for $x \neq x_1,x_2$, treating the soft and hard polymeric segments separately significantly simplifies the mathematical structure. That is, in each segment κ is space-independent, such that except at the discontinuity points, eqn (8) reads

$$\kappa(x)w_q''(x) = \lambda_q w_q(x), \text{ for } \quad \mathfrak{L}^{(1)}, \tag{9}$$

$$\kappa(x)w_q''''(x) = \lambda_q w_q(x), \quad \text{for} \quad \mathfrak{L}^{(2)}. \tag{10}$$

It is thus natural to write the solution separately for the different segments. For each segment, we write $w_q(x)$ as a superposition of the independent solutions of eqn (9) and (10). For $\mathfrak{L}^{(1)}$, the solution of eqn (9) reads

$$w_q(x) = \begin{cases} A_1\cos(qx) + A_2\sin(qx) & 0 < x < x_1 \\ A_3\cos(\tilde{q}x) + A_4\sin(\tilde{q}x) & x_1 < x < x_2 \\ A_5\cos(qx) + A_6\sin(qx) & x_2 < x < L \end{cases}, \tag{11}$$

where A_i are yet undetermined real amplitudes. We also impose the supplementary condition

$$q^2\kappa_\mathrm{h} = \tilde{q}^2\kappa_\mathrm{s} \quad \text{or equivalently} \quad \tilde{q} = \Delta q, \tag{12}$$

which ensures that eqn (9) is satisfied with the same eigenvalue $\lambda_q = L\kappa_\mathrm{h}q^2 = L\kappa_\mathrm{s}\tilde{q}^2$ at all points in space. A mode with negative q can be obtained by rearranging the coefficients $\{A_i\}$ in the corresponding mode with a positive q, so we only consider modes with $q > 0$. Similarly, for $\mathfrak{L}^{(2)}$ we write the solution $w_q(x)$

of eqn (10) as a combination of $\cos(qx)$, $\sin(qx)$, $\cosh(qx)$ and $\sinh(qx)$, with the supplementary condition

$$q^4\kappa_h = \tilde{q}^4\kappa_s \quad \text{or equivalently} \quad \tilde{q} = \Delta q. \tag{13}$$

Note that Δ is defined differently for the two operators, *cf.* eqn (6).

3.2 Internal boundary conditions

A crucial step in calculating the structure of the eigenmodes is specifying the internal boundary conditions (BC) at the discontinuity points $x = x_1, x_2$. These, together with the external boundary conditions at $x = 0$ and $x = L$ determine the amplitudes $\{A_i\}$. It is important to stress that the external boundary conditions completely and uniquely specify the Sturm–Liouville problem. However, since we treat the problem separately for the different segments, we also need to specify the internal BC at the mechanical discontinuity points. That is, the internal BC are a result of our choice to divide the problem into 3 distinct segments. If κ were to change over a finite length-scale, then this division would not have been necessary (nor possible) and no internal BC would have been needed. Such a calculation is carried out in the ESI,† though in this case it cannot be carried out analytically.

The form of the internal BC can be obtained either by taking the limit of an infinitely small variation length of κ, or equivalently, in the following manner. The spatiotemporal dynamics of the system are governed by the equation

$$\mathscr{T}\{w(x,t)\} = \mathfrak{L}\{w(x,t)\}, \tag{14}$$

where $\mathscr{T}$ is a differential operator acting on the time coordinate. $\mathscr{T}\{w(x,t)\}$ is proportional to $\partial_{tt}w(x,t)$ in inertial systems, to $\partial_t w(x,t)$ in highly overdamped systems and might have a more complicated structure in other cases. Since the particular form of $\mathscr{T}$ is irrelevant to this discussion, we do not specify it here. We integrate eqn (14) over a region of size δ around a discontinuity point, say x_1. That is, we consider the region $-\delta < x - x_1 < \delta$ and take the limit $\delta \to 0$. Using the fact that for $x \neq x_1$ κ is space-independent, the integration can be done explicitly. For $\mathfrak{L}^{(1)}$ the result is

$$\lim_{\delta\to 0}\int_{x_1-\delta}^{x_1+\delta}\mathscr{T}\{w(x,t)\}\mathrm{d}x = -L\lim_{\delta\to 0}\left[\kappa_s w'|_{x=\delta} - \kappa_h w'|_{x=-\delta}\right].$$

Irrespective of the explicit form of $\mathscr{T}$, we know that it does not produce a singularity at $x = x_1$ and thus the left-hand-side of the above equation vanishes. We therefore conclude that the function $\kappa(x)w'(x)$ is continuous across the interface. Repeating this procedure again shows that $w(x)$ is continuous across $x = x_1$. As before, one uses the fact that although κ is discontinuous, it is not singular and its integral over a vanishingly small region vanishes.

To summarize, the 4 internal boundary conditions for $\mathfrak{L}^{(1)}$ are

$$[\![w]\!]_{x_1} = [\![w]\!]_{x_2} = [\![\kappa w']\!]_{x_1} = [\![\kappa w']\!]_{x_2} = 0, \tag{15}$$

where $[\![\cdot]\!]_{x_i}$ denotes the jump of a given quantity at $x = x_i$. In particular, as $\kappa(x)$ is discontinuous at x_1 and x_2, $w'(x)$ experiences jump-discontinuity at these points. The somewhat formal derivation of the internal BC at x_1 and x_2 presented above has a clear physical meaning that could have been invoked *a priori*; at any discontinuity of the linear elastic modulus κ, the polymer retains its integrity, *i.e.* $w(x)$ is continuous, and the stress (either torsional or extensional) is continuous, *i.e.* $\kappa(x)w'(x)$ is continuous.

Similarly, for $\mathfrak{L}^{(2)}$ one obtains that the internal boundary conditions at the discontinuity points are

$$[\![w]\!] = [\![w']\!] = [\![\kappa w'']\!] = [\![\kappa w''']\!] = 0. \tag{16}$$

The last two conditions physically correspond to continuity of the mechanical torque and shear force in the polymer.

3.3 The spectrum of permissible wavenumbers q_n

The boundary conditions specified above are all linear and therefore can be summarized concisely in a matrix equation:

$$\boldsymbol{M}(q;\Delta,x_1,x_2)\vec{A} = 0, \tag{17}$$

where $\vec{A}$ is the vector of amplitudes and $\boldsymbol{M}$ is a matrix which can be explicitly calculated. In order to satisfy the boundary conditions simultaneously one must demand $\det\boldsymbol{M} = 0$. The resulting equation can be solved numerically to find the discrete set of permissible q's. For each permissible q, the eigenvectors are easily found by calculating the kernel of the matrix.

For example, the equation that defines the permissible q's for $\mathfrak{L}^{(1)}$ explicitly reads

$$\begin{aligned} 0 \;=\; & \left(\frac{\Delta+1}{\Delta-1}\right)^2\cos[q((x_2-x_1)(\Delta-1)+L)] \\ & + \frac{(\Delta+1)}{(\Delta-1)}\cos[q((x_2-x_1)\Delta-(x_2+x_1)+L)] \\ & - \frac{(\Delta+1)}{(\Delta-1)}\cos[q(-(x_2-x_1)\Delta-(x_2+x_1)+L)] \\ & - \cos[q((x_1-x_2)(1+\Delta)+L)]. \end{aligned} \tag{18}$$

This equation can be solved numerically and the first few modes of $\mathfrak{L}^{(1)}$ and $\mathfrak{L}^{(2)}$ are shown in Fig. 2 and briefly discussed in its caption.

The challenge now is to estimate how the permissible q values are distributed as a function of the parameters. To this end, we numerically solve eqn (18) for some range of inclusion parameters. In Fig. 3 we plot the numerically found wavenumbers $\{q_n\}$ as a function of their ordinal number n, when x_2 is varied while x_1 and Δ are fixed. It is seen that for each fixed set of parameters the spectrum is quasilinear, *i.e.* that one can approximately write the n-th wave number as

$$q_n \approx \frac{C(\Delta,x_1,x_2)}{L}n. \tag{19}$$

Simple dimensional analysis of eqn (18) shows that C can neither depend on L nor on κ_h or κ_s, except through their ratio Δ^2.

How can we estimate $C(\Delta,x_1,x_2)$? The defining equation, eqn (18), is a sum of sinusoidal functions with different frequencies. One can conjecture that the highest frequency, $(\Delta-1)(x_2-x_1)+L$, is the one that controls the density of solutions. This argument predicts that the equation for C should read

$$C \simeq \frac{\pi L}{(\Delta-1)(x_2-x_1)+L} = \frac{\pi}{\phi\Delta+1-\phi}. \tag{20}$$

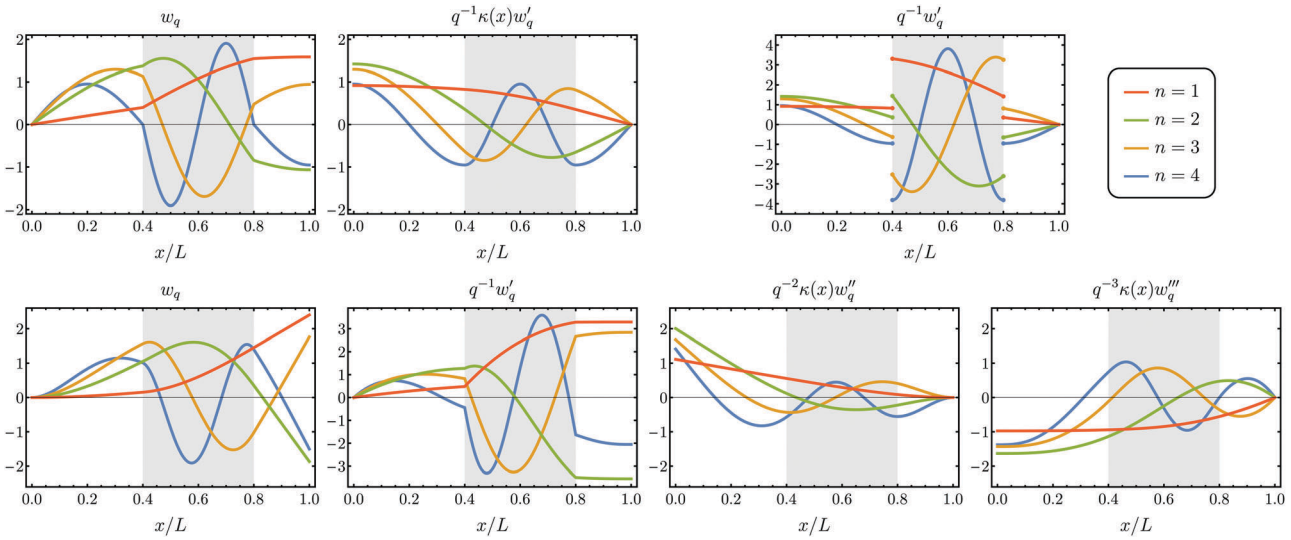

Fig. 2 Lowest 4 modes of $\mathfrak{Q}^{(1)}$ (top row) and $\mathfrak{Q}^{(2)}$ (bottom row) and their derivatives. The leftmost panels show the modes and successive panels show successive derivatives. In cases where the derivatives are discontinuous we plot the derivatives multiplied by the discontinuous $\kappa(x)$, which results in continuous functions, *cf.* eqn (15) and (16). As an example, the rightmost panel in the top row shows w' itself, explicitly demonstrating the discontinuity. The parameters used here and in what follows are $x_1 = 0.4L$, $x_2 = 0.8L$ and $\Delta = 1.5$. The shaded area shows the region in space where $\kappa(x) = \kappa_s$ and it is readily seen that in this region the wavelength of the modes is shorter.

Fig. 3 demonstrates a numerical verification of this prediction. Note that C depends on x_1 and x_2 only through their normalized difference ϕ, *i.e.* C does not depend on the location of the inclusion but only on its relative size. In fact, the same relation holds also if two or more inclusions are present. In this case C depends on the total fraction of the polymer which is occupied by the inclusions (not shown). For the operator $\mathfrak{Q}^{(2)}$, the analysis is similar yet more technically involved. The final result, though, is identical – the wavenumber of the n-th eigenmode is quasi-linear in n and the proportionality factor is given by eqn (20) (although the definition of Δ is different, *cf.* eqn (6)). Lastly, we note that the case of a homogeneous polymer, *i.e.* $C = \pi$, is readily recovered for $\Delta = 1$ or $\phi = 0$.

The constant C provides a closed-form, non-perturbative approximation for the structure of the spectrum of $\mathfrak{Q}$. It can also be derived heuristically using the following reasoning. Writing the denominator of C as $\phi\cdot\Delta + (1 - \phi)\cdot 1$, it is seen that it is a rule of mixture between Δ and 1, with relative weights of ϕ and $1 - \phi$, respectively. In the spirit of eqn (11)–(13), an eigenmode of either $\mathfrak{Q}^{(1)}$ or $\mathfrak{Q}^{(2)}$ can be written schematically as

$$w_q(x) \sim \begin{cases} e^{iqx} & \text{in the stiff regions} \\ e^{iq\Delta x} & \text{in the soft regions} \end{cases}. \qquad (21)$$

Thus, if we "stretch" the x coordinate in the softer regions by an amount Δ, the eigenmode will have the same wavenumber in

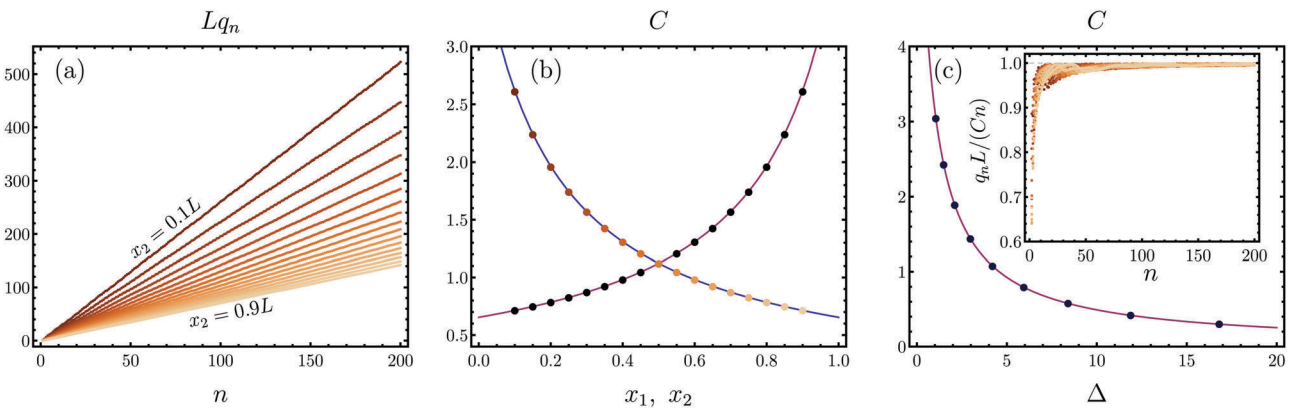

Fig. 3 (a) The numerically found q values of $\mathfrak{Q}^{(1)}$ as a function of their ordinal number for fixed $x_1 = 0.05L$ and $\Delta = 5$. Different colors correspond to different values of x_2 which varies at constant steps between $0.1L$ and $0.9L$. (b) Colored data points show the slopes of the data in panel (a) as a function of x_2 (following the same color code), and the solid line is the prediction of eqn (20). The black data are obtained using the same procedure, but when $x_2 = 0.95L$ is fixed and x_1 varies. (c) The same as (b), but now Δ is varied and $x_1 = 0.2L$, $x_2 = 0.8L$ are fixed. Inset: The same data and color code as in panel (a), normalized by the predicted value Cn. It is seen that the ratio exhibits significant deviations from unity only for the first few modes.

both regions. That is, if we define a new variable $\tilde{x}$ by the differential $\mathrm{d}\tilde{x} \equiv \sqrt{\kappa_h/\kappa(x)}\mathrm{d}x$ for $\mathfrak{L}^{(1)}$ and $\mathrm{d}\tilde{x} \equiv \sqrt[4]{\kappa_h/\kappa(x)}\mathrm{d}x$ for $\mathfrak{L}^{(2)}$, then $w(\tilde{x})$ has the same wavenumber in all points along the polymer. However, it is not a pure sinusoidal function because of the jump conditions at the mechanical discontinuity points x_1 and x_2, *cf.* eqn (15) and (16). Thus, in terms of the variable $\tilde{x}$ the eigenmodes are those of a uniform system with some jump conditions on the derivative. This is analogous, though not strictly equivalent, to the problem of a vibrating uniform string of length $\tilde{L} \equiv L(\phi\cdot\Delta + (1-\phi)\cdot 1)$, with massive beads attached at the discontinuity points. For the latter, it is quite intuitive that $q_n \simeq n\pi/\tilde{L}$, which is the result of eqn (20). Note that this heuristic derivation also rationalizes the fact that C does not depend on the position of the inclusion within the polymer but only on its size $x_2 - x_1$. More generally, for a polymer with multiple soft regions C will depend only on the total fraction of the polymer occupied by the softer regions.

Eqn (19) and (20), together with the relation between λ_q and q_n, provide an analytical description of the spectrum of eigenvalues in the framework of the continuum theory, which is the major result of this section. In the next section, the corresponding discrete problem is solved.

4 Eigenmode analysis: discrete theory

In the preceding section the continuum eigenmode problem was formulated and solved. Here the same problem is addressed within the corresponding discrete theory, in order to highlight the similarities and the discrepancies between the two approaches. Our goal then is to find the eigenmodes $\vec{w}_q$, and their associated eigenvalues λ_q, that satisfy $\boldsymbol{H}\vec{w}_q = \lambda_q\vec{w}_q$. As before, we assume the eigenmodes to be sinusoidal with different wavelengths in the different regions. That is, we write the discrete analog of eqn (11), where the k-th component of $\vec{w}_q$ is given by

$$\{w_q\}_k \sim \begin{cases} e^{iqka} & \text{in the stiff regions} \\ e^{i\tilde{q}ka} & \text{in the soft regions} \end{cases}. \tag{22}$$

For a homogeneous chain it is well known,[21] and easily verified, that this results in a sinusoidal dispersion relation,

$$\begin{aligned} \lambda(q) &= \kappa\left[2\sin\left(\frac{qa}{2}\right)\right]^2 \quad \text{for } \boldsymbol{H}^{(1)}, \\ \lambda(q) &= \kappa\left[2\sin\left(\frac{qa}{2}\right)\right]^4 \quad \text{for } \boldsymbol{H}^{(2)}. \end{aligned} \tag{23}$$

The allowed wavenumbers for homogeneous systems with the chosen boundary conditions are

$$q_j a = \pi\frac{j-\frac{1}{2}}{N+\frac{1}{2}}, \quad j = 1,\ldots,N. \tag{24}$$

Since the eigenvalue equation $H_{ij}w_j = \lambda(q)w_i$ must be satisfied with the same eigenvalue at all points, the relation between q and $\tilde{q}$ (*i.e.* the discrete analog of eqn (12) and (13)) reads $\lambda(q) = \lambda(\tilde{q})$. This implies

$$\Delta\sin\left(\frac{qa}{2}\right) = \sin\left(\frac{\tilde{q}a}{2}\right) \Rightarrow \tilde{q} = \frac{2}{a}\sin^{-1}\left[\Delta\sin\left(\frac{qa}{2}\right)\right], \tag{25}$$

valid for both $\boldsymbol{H}^{(1)}$ and $\boldsymbol{H}^{(2)}$. This identifies with eqn (12) and (13) to leading order in qa, but differs substantially for qa of order unity. Specifically, the sinusoidal functions can give rise to complex wavenumbers at high qa, that is, to (partially) evanescent eigenmodes. It is important to stress that this is a fundamental difference between the discrete and the continuum theories and that the discrete evanescent eigenmodes do not have a continuum counterpart. Physically, this happens because $\tilde{q} > q$ and therefore it might happen that at high q the wavelength in the hard region is larger than the monomeric size a (and thus is allowed), while the wavelength in the soft region is shorter than a, and will thus be evanescent. One can see this explicitly by thinking of eqn (25) as an implicit function defining $\tilde{q}$ in terms of q. As q grows, $\tilde{q}$ grows faster but this can only happen before the left-hand-side of eqn (25) reaches unity. For higher values of q there exists no real solution for $\tilde{q}$. The transition occurs exactly when $\tilde{q}a = \bar{\pi}$, *i.e.* when the wavelength in the soft region is comparable to the monomeric size.

The existence of these evanescent high-q modes is numerically verified, as shown in Fig. 4 along with the full spectrum. It is seen that the spectrum consists of two parts separated by a sharp boundary. This boundary corresponds exactly to the division between evanescent and non-evanescent modes and it occurs at a critical wavenumber q_c which satisfies $q_c a = 2\sin^{-1}(\Delta^{-1})$, as predicted by eqn (25). In fact, for the evanescent modes q_n is linear in n, with a slope that identifies with that of a homogeneous chain, *cf.* eqn (24), when N is replaced by the number of sites in the hard region, $N(1-\phi)$.

The relative amplitudes of the modes in the soft and hard segments are obtained by imposing continuity requirements at x_1 and x_2, which are the discrete analogs of eqn (15) and (16) and are not written here for brevity. Irrespective of the particular form of these conditions, they clearly imply that a mode that decays exponentially for $x > x_1$ will have vanishingly small amplitude in the hard region $x > x_2$ and *vice versa*. That is, the evanescent modes are localized in either of the two hard regions, but not both, except in some degenerate cases. This result, which manifestly holds also for polymers with more than one soft region, is clearly seen in the inset of Fig. 4. In addition, since the imaginary part of $\tilde{q}$ is a rapidly increasing function of q (grows as $\sqrt{q-q_c}$), the evanescence length of the modes rapidly shrinks with increasing q, as is also seen in Fig. 4.

With this, the eigenmode analysis in the framework of both the continuum and discrete theories is completed. Next, the statistical thermodynamic implications of the obtained results are explored.

5 Statistical thermodynamics

The statistical theory of fluctuating polymers has been intensively studied in the literature in various contexts.[4,5,22] Our goal here,

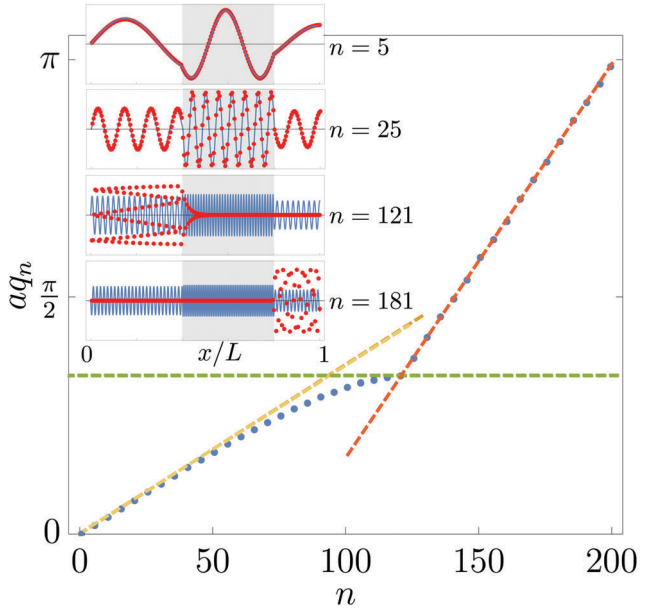

Fig. 4 Spectrum of the discrete operator $\boldsymbol{H}^{(1)}$. Main panel: the nth wavevector q_n as a function of the ordinal number n. q_n is obtained from the numerically calculated λ_n by means of eqn (23). For clarity, only every 5th value is plotted. The orange line shows the continuum prediction of eqn (19) and (20). The slope of the dashed red line corresponds to a homogeneous chain of length $(1-\phi)N$ (see text). The green line shows the value $\Delta \sin\left(\frac{qa}{2}\right) = 1$, above which no real solution for $\tilde{q}$ exists, *cf.* eqn (25). Insets: A few selected eigenmodes (continuum theory in blue, discrete theory in red). It is seen that at low q the agreement between the continuum and discrete theories is perfect, and that at higher q discrepancies emerge. The discrete 121th eigenmode is the first evanescent eigenmode, with visible exponential decay in the soft region $x > x_1$, *i.e.* $\tilde{q}$ is complex. The discrete 181th eigenmode is localized in the other hard segment, $x > x_2$, with an evanescence length of monomeric size.

following the analysis of the previous sections, is to understand the effect of spatial inhomogeneity on these fluctuations[6,8] and to elucidate the differences between the continuum and the discrete approaches to the problem. Specifically, we will address the dependence of thermodynamic quantities (mainly the free-energy) on the properties of the inclusion (*i.e.* ϕ and Δ) and on external geometric constraints, along with the associated fluctuation-induced forces.

A crucial player in theories of Gaussian thermal fluctuations is the eigenmode spectrum of the relevant dynamical operator. These spectra were analytically calculated in the preceding sections for both the continuum dynamical operator and its discrete counterpart. These calculations fully take into account the internal spatial inhomogeneity of the polymer, quantified by the normalized size ϕ and strength Δ of the inclusion. In addition, in order to account for prototypical external constraints, we focus on extensional fluctuations (*i.e.* those governed by $U^{(1)}$), which are constrained by a rigid wall. Specifically, the relative elongation (strain) of the polymer is restricted to be smaller than ε, or equivalently, that its length is bounded to be smaller than $L(1+\varepsilon)$. In the limit $\varepsilon \to \infty$ the fluctuations are unconstrained, while otherwise the available configurations are constrained, which should be explicitly taken into account in thermal averages. In particular, if the field $w(x)$ is rendered dimensionless by measuring lengths in terms of L, the constraint is expressed mathematically by imposing $w_N < \varepsilon$ in the discrete description and $w(L) < \varepsilon$ in the continuous one. Since the results are qualitatively similar for both operators $U^{(1)}$ and $U^{(2)}$, we perform this analysis only for $U^{(1)}$, as stated above. Moreover, while for a strong confinement the constraint generically results in coupling between the bending, twisting and extensional dynamics, this coupling will be small for short polymers like those we consider (*i.e.* of length comparable to the persistence length) and since the emphasis of this work is on the effects of inhomogeneity we do not consider this coupling here.

The main thermodynamic quantity of interest, from which all statistical thermodynamic properties follow, is the partition function $\mathscr{Z}$. The parameters ϕ, Δ and ε affect $\mathscr{Z}$ in two distinct ways: the internal constraints, *i.e.* the properties of the inclusion ϕ and Δ, affect the dynamical operator (and thus its spectrum) directly, while the external constraint ε enters by restricting the allowed configurations over which the thermal average is performed. Explicitly, the partition function $\mathscr{Z}$ is given by the functional integral

$$\mathscr{Z} = \int Dw \exp[-\beta\langle w|\mathfrak{D}(\phi,\Delta)|w\rangle]\Theta(\varepsilon - w(L)), \qquad (26)$$

where $\beta \equiv (k_B T)^{-1}$, k_B is Boltzman's constant, Θ is Heaviside's step function and $\mathfrak{D}$ is the dynamic operator, *i.e.* either $\mathfrak{L}$ or $\boldsymbol{H}^{(1)}$ (in the discrete calculation $w(L)$ should be replaced by w_N). For quadratic energy functionals, which is the subject of the present discussion, the partition function $\mathscr{Z}$ can be explicitly calculated in terms of Gaussian integrals. The calculation itself is rather straightforward, yet laborious. The details are given in the ESI† and here we only discuss the final result in which the free-energy is expressed as

$$F \equiv -k_B T \log \mathscr{Z} = F_{uc}(\phi,\Delta) + F_{\varepsilon}(\varepsilon,\phi,\Delta), \qquad (27)$$

where F_{uc} is the free-energy of the unconstrained chain (*i.e.* F for $\varepsilon \to \infty$) and F_{ε} is the contribution associated with the external constraint ε. Below we study each of these contributions separately.

5.1 Unconstrained free-energy

The unconstrained free-energy can be expressed in terms of the eigenvalues as (see ESI† for details)

$$F_{uc} = \frac{k_B T}{2}\log\left[\frac{\det \mathfrak{D}}{(k_B T)^N}\right] = \frac{k_B T}{2}\sum_q \log\left(\frac{\lambda_q}{k_B T}\right). \qquad (28)$$

Equipped with an approximate expression for the eigenvalues of $\mathfrak{L}^{(1)}$ and an analytical expression for $\det \boldsymbol{H}^{(1)}$, the above formula can be evaluated explicitly.† The result, after taking the large-N limit, reads

$$F_{uc}^{DT} = N k_B T\left[\frac{1}{2}\log\left(\frac{\beta\kappa_h}{L/N}\right) - \phi\log\Delta\right],$$

$$F_{uc}^{CT} = N k_B T \times \left[\frac{1}{2}\log\left(\frac{\beta\kappa_h}{L/N}\right) - \log(\phi\Delta + 1 - \phi) + \log\left(\frac{\pi\sqrt{N}}{e}\right)\right]. \qquad (29)$$

Here and in what follows the superscript DT stands for "Discrete theory", *i.e.* the results pertaining to $\boldsymbol{H}^{(1)}$, and CT for "Continuum theory", *i.e.* the results pertaining to $\mathfrak{L}^{(1)}$.

To gain more insight into the structure and physical content of eqn (29), we rewrite the unconstrained free-energy as the sum of the free-energies of the homogeneous segments and an interaction energy. That is, we write

$$F_{\rm uc} = N(\phi f(\kappa_{\rm s}) + (1-\phi) f(\kappa_{\rm h})) + F_{\rm int}, \qquad (30)$$

for both theories, where $f(\kappa)$ is the specific (per monomer) free-energy of a homogeneous polymer with modulus κ, and $F_{\rm int}$ is the interaction energy between the soft and hard segments. This form of writing is common in the context of calculating Casimir-like fluctuation-induced forces between inclusions,[23–25] to be discussed below. In this representation, we need to calculate the homogeneous polymer free-energies in the two theories, which take the form:†

$$\begin{aligned} f^{\rm DT}(\kappa) &= \frac{1}{2} k_{\rm B}T \log\left(\frac{\beta\kappa}{a}\right), \\ f^{\rm CT}(\kappa) &= \frac{1}{2} k_{\rm B}T \log\left(\frac{\beta\kappa}{a}\right) + k_{\rm B}T \log\left(\frac{\pi\sqrt{N}}{e}\right). \end{aligned} \qquad (31)$$

We note that the two theories agree quantitatively on the specific free-energy, up to a logarithmic factor in N. The latter actually implies that the free-energy in the continuum theory is not strictly extensive, an issue that pertains already to the continuum theory of homogeneous systems and is not discussed here. Eqn (29)–(31) indicate that the interaction energy in the two cases reads

$$F_{\rm int}^{\rm DT} = 0, \quad F_{\rm int}^{\rm CT} = N k_{\rm B}T \log\left(\frac{\Delta^{\phi}}{\phi\Delta + (1-\phi)}\right), \qquad (32)$$

revealing fundamental differences between the two theories. This non-trivial result means that the discrete theory predicts the free-energy of an inhomogeneous polymer to be simply the sum of the free-energies of the soft and hard regions without any interaction. In fact, this holds for an arbitrary choice of κ_i, not necessarily the hard-soft-hard configuration described here.† In contrast, the continuum theory predicts a non-trivial dependence of the free-energy on the inclusion parameters. The analytical results in eqn (27)–(32) are all corroborated against explicit numerical calculations, as shown in Fig. 5.

This discrepancy in the free-energy can be manifested in measurable quantities, such as the configurational contribution to the fluctuation-induced force $\partial_\phi F$. Physically, this force corresponds – *e.g.* in the case of cofilin-mediated softening of actin filaments, where local softening of the actin polymer is induced by the adsorption of cofilin molecules from the solvent[10] – to the fluctuation-induced contribution to an adsorption force. The latter also includes other contributions, *e.g.* the binding energy, the change in the solvent mixing entropy and the entropy associated with placing the inclusion at different locations along the polymer, which are of no interest in the present context.

As we focused here on the unconstrained free-energy $F_{\rm uc}$, we calculate first $\chi_\phi \equiv \partial_\phi F_{\rm uc}$, which takes the form

$$\chi_\phi^{\rm DT} = -N k_{\rm B}T \log\Delta, \quad \chi_\phi^{\rm CT} = -N k_{\rm B}T \frac{\Delta - 1}{(\Delta-1)\phi + 1}. \qquad (33)$$

Later on we will show that the contribution of F_ε to this force, $\partial_\phi F_\varepsilon$, is the same for both theories. $\chi_\phi^{\rm DT}$ and $\chi_\phi^{\rm CT}$ of eqn (33) agree

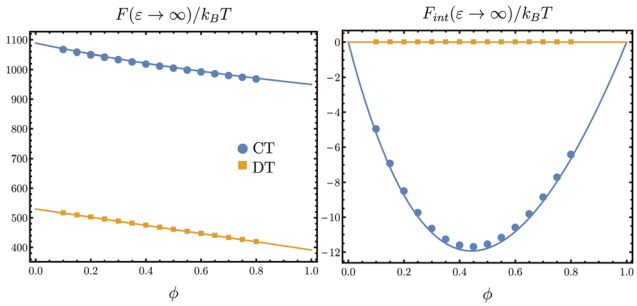

Fig. 5 The total free-energy (left) and the interaction free-energy (right) as a function of ϕ for $\varepsilon \to \infty$. The solid lines show the analytical predictions of eqn (27)–(32) and the data points correspond to direct numerical calculations. The small negative deviation of the continuum theory prediction for $F_{\rm int}$ from the numerical results emerges from using Stirling's approximation, which can be eliminated by taking higher order corrections (not shown).

only in the limit of very small mechanical contrast, $\Delta \to 1$, but otherwise significantly differ, highlighting a stark discrepancy between the continuum and discrete theories. This discrepancy will be extensively discussed in Section 6. Before that, we study the free-energy associated with the external constraint ε and see whether similar discrepancies persist there too.

5.2 External-constraint-related free-energy

The contribution of the external constraint to the free-energy, F_ε, can be explicitly calculated† and takes the form

$$F_\varepsilon = k_{\rm B}T \log\left[1 + \mathrm{erf}\left(\varepsilon\sqrt{\frac{\beta\kappa_{\rm eff}(\phi,\Delta)}{2L}}\right)\right]. \qquad (34)$$

This expression for F_ε is valid for both the continuum and discrete theories, where the effective modulus that depends on the inclusion parameters $\kappa_{\rm eff}(\phi,\Delta)$ takes the form

$$\begin{aligned} \kappa_{\rm eff}^{\rm DT}(\phi,\Delta) &= \left(\frac{\phi}{\kappa_{\rm s}} + \frac{1-\phi}{\kappa_{\rm h}}\right)^{-1} = \frac{\kappa_{\rm h}}{\phi\Delta^2 + (1-\phi)}, \\ \kappa_{\rm eff}^{\rm CT}(\phi,\Delta) &= \kappa_{\rm h}\left[\sum_q \left(\frac{u_q(L)}{qL}\right)^2\right]^{-1}, \end{aligned} \qquad (35)$$

in the two theories. erf(·) in eqn (34) is the error function. Note that for a homogeneous polymer, *i.e.* $\Delta = 1$ or $\phi = 0$, $\kappa_{\rm eff}^{\rm DT}$ identifies with the bare modulus of the polymer.

Since the two theories predict the same functional form for F_ε, differences between them can emerge only due to possible differences between $\kappa_{\rm eff}^{\rm DT}$ and $\kappa_{\rm eff}^{\rm CT}$. We thus need to compare these two. $\kappa_{\rm eff}^{\rm DT}$ in eqn (35) is exactly the effective macroscopic κ of a chain of microscopic springs connected in series. To better understand $\kappa_{\rm eff}^{\rm CT}$ and its relation to $\kappa_{\rm eff}^{\rm DT}$, we define $\kappa_n^{\rm CT}$ as the partial sum over eigenmodes

$$\kappa_n^{\rm CT} = \kappa_{\rm h}\left[\sum_{i=1}^{n}\left(\frac{u_{q_i}(L)}{q_i L}\right)^2\right]^{-1}. \qquad (36)$$

In this way we can quantify the contribution of eigenmodes of increasing wavenumber to $\kappa_{\rm eff}^{\rm CT}$. In Fig. 6c we plot the deviation of $\kappa_n^{\rm CT}/\kappa_{\rm eff}^{\rm DT}$ from unity as a function of the number of modes n.

It is observed that κ_n^{CT} converges to the discrete theory prediction $\kappa_{\mathrm{eff}}^{\mathrm{DT}}$ after summation over a sub-extensive number of modes. That is, the two theories essentially predict the same effective modulus κ_{eff} and consequently the same F_ε. This agreement, contrasted with the discrepancy in the two predictions for F_{uc}, will be discussed in Section 6.

Before concluding this subsection, let us briefly comment on the structure of F_ε, which has a neat physical interpretation. Let us consider the internal energy $U_\varepsilon = -\partial_\beta(\beta F_\varepsilon)$ (which is the same for both the continuum and discrete approaches), which reads

$$\beta U_\varepsilon(\xi) = -\frac{\mathrm{e}^{-\xi^2}\xi}{\sqrt{\pi}[1+\mathrm{erf}(\xi)]}, \tag{37}$$

where the notation $\xi \equiv \varepsilon\sqrt{\frac{\beta\kappa_{\mathrm{eff}}}{2L}}$ was introduced. We note that the internal energy associated with the unconstrained free-energy, $\partial_\beta(\beta F_{\mathrm{uc}})$, trivially equals $\frac{1}{2}Nk_{\mathrm{B}}T$ according to the equipartition theorem. Consequently, U_ε in fact measures the deviation of the internal energy from the background thermal energy predicted by equipartition.

In the limit of large ξ, $U_\varepsilon(\xi)$ vanishes, as expected (*i.e.* the polymer is essentially unconstrained). In the limit of large negative ξ (note, though, that ε is physically bounded from below by -1), we have

$$U_\varepsilon(\xi \to -\infty) \simeq k_{\mathrm{B}}T\left(\xi^2 + \frac{1}{2}\right) = \frac{\kappa_{\mathrm{eff}}}{2L}\varepsilon^2 + \frac{k_{\mathrm{B}}T}{2}. \tag{38}$$

In this limit, the polymer is under compression and responds predominantly elastically, *i.e.* its internal energy varies as ε^2 with a prefactor is proportional to the effective modulus κ_{eff}. Note that the ordinary compression-extension elastic symmetry, *i.e.* symmetry under $\varepsilon \to -\varepsilon$ ($\xi \to -\xi$), is broken here since the confining wall is not attached to the polymer. All of the properties of $U_\varepsilon(\xi)$ are shown in Fig. 6a. When ξ is not very negative F_ε is entropic in nature and vanishes for $T \to 0$ (recall that the persistence length of a homogeneous polymer is $\beta\kappa$, hence the factor $\frac{\beta\kappa_{\mathrm{eff}}}{2L}$ can be interpreted as the number of times the effective persistence length enters in the size of the polymer).

The thermodynamic force related to the external constraint, $\chi_\varepsilon \equiv \partial_\varepsilon F$, is a measurable physical quantity (*e.g.* the pressure on a confining wall) that can also be calculated. It is plotted in Fig. 6b, where it is seen that for negative values of ε near -1 it is linear and its origin is predominantly elastic, as expected from the preceding discussion, while it decays to zero when $\varepsilon \to \infty$. For intermediate positive values it is a fluctuation-induced force and the transition between the elastic and fluctuation-induced regimes is not sharp, but is rather smoothed by temperature. Clearly, for $T \to 0$ the force is strictly linear at $\varepsilon < 0$ and strictly vanishes for $\varepsilon > 0$.

Next, we turn to discuss the relation between the continuum and discrete theories in the light of the results obtained up to now.

6 Validity of the continuum theory

In the previous section we saw that various statistical thermodynamic properties of inhomogeneous polymers reveal significant differences between the continuum and discrete theories. That is, the interaction free-energy between the soft and hard segments in eqn (32) and the fluctuation-induced adsorption force in eqn (33) feature qualitative discrepancies between the continuum and discrete theories, except for the small contrast limit $\Delta \to 1$, where $F_{\mathrm{int}}^{\mathrm{CT}} \approx F_{\mathrm{int}}^{\mathrm{DT}} = 0$ and $\chi_\phi^{\mathrm{CT}} \approx \chi_\phi^{\mathrm{DT}} \sim \Delta - 1$. In particular, $F_{\mathrm{int}}^{\mathrm{DT}} = 0$ identically, while its continuum counterpart is a non-trivial function of ϕ and Δ, *cf.* eqn (32). A corollary is

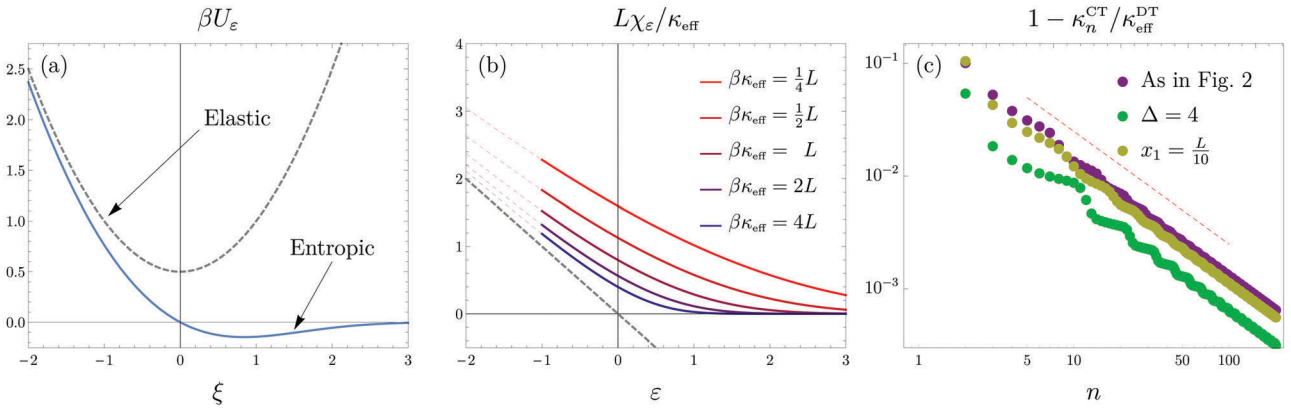

Fig. 6 (a) The internal energy U_ε related to the external constraint ε (solid line), *cf.* eqn (37), and the elastic energy with effective modulus κ_{eff} (dashed line), *cf.* eqn (38), as a function of the dimensionless coordinate ξ. The elastic energy is plotted also for $\xi > 0$, corresponding to extension, though no elastic behavior is physically observed in this regime as the confining wall is not attached to the polymer. (b) The thermodynamic force χ_ε as a function of ε for varying values of the dimensionless combination $\beta\kappa_{\mathrm{eff}}/L$. While results for $\varepsilon < -1$ are outside of the physically accessible range and hence are plotted as thin dashed lines, they provide good approximations to the behavior of the free-energy in the physical range $\varepsilon \gtrsim -1$. (c) The convergence of the continuum theory prediction for κ_{eff} towards the discrete theory prediction of eqn (35). The plot shows the relative deviation $1 - \kappa_n^{\mathrm{CT}}/\kappa_{\mathrm{eff}}^{\mathrm{DT}}$, where the partial sum κ_n^{CT} is defined in eqn (36), as a function of the number of summed eigenmodes n. The purple data correspond to the same parameter values used throughout the paper, *e.g.* Fig. 2, and other colors correspond to one parameter being changed each time, as stated in the legend. It is observed that a convergence to within 1% is achieved after summing over the first $\sim$10 modes for all parameters tested.

that χ_ϕ^{CT} depends on ϕ, while χ_ϕ^{DT} is independent of it, *cf.* eqn (33). We stress that these discrepancies are not mitigated when the discretization length is taken to zero, when a different ultra-violet cutoff is used or when the variation of $\kappa(x)$ is smoothed out.† What can one make of these discrepancies?

Obviously, the continuum analysis of the eigenmodes and eigenvalues of the inhomogeneous polymer, which is the basis for any statistical thermodynamic calculation in the Gaussian approximation, is strictly valid only for small wavenumbers $qa \ll 1$. This is true in general and has been analytically demonstrated in Sections 3 and 4, revealing qualitative differences in the eigenmode and eigenvalue spectra of the continuum and discrete operators at large wavenumbers. This by itself does not invalidate the continuum approach. The pertinent question then is whether a given physical observable is dominated by small wavenumbers, in which case the continuum approximation is valid.

The results of Section 5 indicate that this is not the case. Beyond the directly observed differences between the continuum and discrete results themselves, this can be inferred from the continuum result alone. Let us go back to eqn (30); the first two contributions to the (unconstrained) free-energy on the right-hand-side are "bulk" contributions, *i.e.* terms that scale with the total size of the soft segment ϕN and the two hard segments $(1-\phi)N$. Since $N \sim L/a \sim Lq_{max}$, where q_{max} is the UV-cutoff, these contributions depend explicitly on the large wavenumbers and in general are not expected to be correctly described by the continuum theory (we note again that the fact that the continuum "bulk" free-energy is not even strictly extensive in our case, *cf.* the second equation in (31), is not discussed here). The important point is that in the thermodynamic limit, where $q_{max} \to \infty$, these "bulk" contributions diverge and are commonly eliminated in standard calculations.[25,28]

We are then left with the last term on the right-hand-side of eqn (30), F_{int}^{CT}, the interaction free-energy between soft and hard segments. The result in eqn (32) shows that the interaction free-energy also scales with $N \sim q_{max}$ and hence depends explicitly on the UV-cutoff, marking the breakdown of the continuum theory in this case. Consequently, the continuum result for the fluctuation-induced adsorption force, χ_ϕ^{CT} in eqn (33), scales with the system size N and is therefore not dominated by small wavenumbers. This should be contrasted with Casimir-like fluctuation-induced forces in which the interaction energy depends on a geometric degree of freedom, *e.g.* the separation between two plates, but is independent of q_{max}.[28,29] In this case, after the divergent "bulk" contributions are removed, a continuum-level fluctuation-induced force is identified by taking the derivative of the interaction free-energy with respect to the geometric degree of freedom. It is important to note that a physically realistic fluctuation-induced adsorption force does exist in our problem and is given by the discrete theory result χ_ϕ^{DT} in eqn (33). In this context, we note that recent works have successfully used continuum theory (utilizing the Green's function approach) to calculate the interaction between imposed bending angle inclusions in a worm-like-chain model.[26,27] Unlike χ_ϕ, the continuum approach does not fail in this case because the Green's function that they use, *i.e.* the response of the polymer to an imposed bending angle at a given point, is not dominated by large q contributions, in line with the current discussion.

The continuum analysis presented above bears some similarity to the Debye model of the specific heat of homogeneous systems. There, similarly to the main panel of Fig. 4, a continuum-level linear spectrum of wavenumbers replaces the nonlinear spectrum of the discrete theory (both agree of course for $qa \ll 1$), keeping the total number of eigenmodes the same. When coupled to the Bose–Einstein statistics for the occupation number the heat capacity features the famous T^3 behavior at low T. There are two major differences between Debye's analysis and ours; first, our analysis was strictly classical, not taking into account quantum effects such as those incorporated into the Bose–Einstein distribution. This makes a difference because the latter provides a physical UV cutoff that at low T assigns negligible weight to the high-q modes for which the continuum theory is invalid. Second, as we explicitly demonstrated, spatial inhomogeneity gives rise to differences between the continuum and discrete eigenmodes/eignevalues, which are not encountered in spatially homogeneous systems.

In contrast to χ_ϕ, the fluctuation-induced force associated with an external constraint – χ_ε derived from F_ε of eqn (34) – does not depend on q_{max} and the continuum and discrete predictions coincide. That is, this fluctuation-induced force is properly described by the continuum theory. The reason for this is that in this case the relevant fluctuations are shape fluctuations, which are dominated by small wavenumbers (since the amplitude of the eigenmodes decays with increasing q). Mathematically speaking, this property is encapsulated in the fact that κ_{eff}^{CT} of eqn (35), which is expressed as a sum over wavenumbers, converges to κ_{eff}^{DT} of eqn (35) after summing over the first few smallest wavenumbers, as shown in Fig. 6.

7 Concluding remarks

In this paper we studied the mechanics and statistical thermodynamics of semiflexible inhomogeneous polymers. We focused on inhomogeneity in the form of a soft inclusion embedded inside a stiffer/harder polymer, and considered torsional, extensional and bending Gaussian fluctuations. The analytical results for the eigenmode and eigenvalue spectra of both the continuum and the corresponding discrete dynamical operators were derived. The analysis revealed qualitative differences between the continuum and discrete spectra. Most notably, it was shown that above a certain wavenumber, the discrete spectrum of wavenumbers q_n changes qualitatively and the discrete modes become evanescent inside the soft inclusion, having no continuum counterparts.

Based on the eigenmode and eigenvalue analysis, we derived explicit expressions for two types of fluctuation-induced forces in the framework of both the continuum and discrete theories. One fluctuation-induced force is associated with variations of the properties of the inclusion, *i.e.* its size and strength. This entropic force describes, for example, the fluctuation-induced contribution to the adsorption of molecules that give rise to the

soft inclusion. Another fluctuation-induced force is associated with an external geometric constraint, *i.e.* a confining wall with variable positions. This entropic force describes the pressure applied by the fluctuating polymer on the wall.

It was shown that the first fluctuation-induced force is dominated by contributions from modes with large wavenumbers, where the continuum and discrete spectra significantly differ, and hence that the continuum theory breaks down. On the other hand, the second fluctuation-induced force was shown to be dominated by small wavenumber shape fluctuations and hence is properly described by the continuum theory. The results show that while the continuum theory of inhomogeneous polymers may be successful in some cases, it fails in others, and should be taken with some caution.

Acknowledgements

We are indebted to S. Safran and O. Farago for very useful discussions. We also thank E. Brener, M. Kardar, N. Gov and P. Pincus for useful comments. E. B. acknowledges support from the Israel Science Foundation (Grant No. 712/12), the Harold Perlman Family Foundation, and the William Z. and Eda Bess Novick Young Scientist Fund.

References

1 M. D. Ediger, *Annu. Rev. Phys. Chem.*, 2000, **51**, 99–128.
2 A. Cavagna, *Phys. Rep.*, 2009, **476**, 51–124.
3 L. Berthier and G. Biroli, *Rev. Mod. Phys.*, 2011, **83**, 587–645.
4 P.-G. De Gennes, *Scaling concepts in polymer physics*, Cornell University Press, 1979.
5 S. A. Safran, *Statistical thermodynamics of surfaces, interfaces, and membranes*, Addison-Wesley, 1994.
6 E. Helfand, *J. Chem. Phys.*, 1975, **62**, 999.
7 Y. O. Popov and A. V. Tkachenko, *Phys. Rev. E: Stat., Nonlinear, Soft Matter Phys.*, 2007, **76**, 021901.
8 T. Su and P. K. Purohit, *J. Mech. Phys. Solids*, 2010, **58**, 164–186.
9 E. Prochniewicz, N. Janson, D. D. Thomas and E. M. De la Cruz, *J. Mol. Biol.*, 2005, **353**, 990–1000.
10 B. R. McCullough, L. Blanchoin, J.-L. Martiel and E. M. De La Cruz, *J. Mol. Biol.*, 2008, **381**, 550–558.
11 O. N. Yogurtcu, J. S. Kim and S. X. Sun, *Biophys. J.*, 2012, **103**, 719–727.
12 V. E. Galkin, A. Orlova, D. S. Kudryashov, A. Solodukhin, E. Reisler, G. F. Schröder and E. H. Egelman, *Proc. Natl. Acad. Sci. U. S. A.*, 2011, **108**, 20568–20572.
13 S. Panyukov and Y. Rabin, *Macromolecules*, 1996, **29**, 7960–7975.
14 D. Bensimon, D. Dohmi and M. Mezard, *Europhys. Lett.*, 1998, **42**, 97.
15 J. Lipfert, S. Klijnhout and N. H. Dekker, *Nucleic Acids Res.*, 2010, **38**, 7122–7132.
16 V. V. Kostjukov and M. P. Evstigneev, *Phys. Rev. E: Stat., Nonlinear, Soft Matter Phys.*, 2012, **86**, 86–88.
17 W. Helfrich, *Z. Naturforsch., C: J. Biosci.*, 1973, **28**, 693–703.
18 M. Kardar, *Statistical physics of fields*, Cambridge University Press, 2007.
19 B. R. McCullough, E. E. Grintsevich, C. K. Chen, H. Kang, A. L. Hutchison, A. Henn, W. Cao, C. Suarez, J.-L. Martiel, L. Blanchoin, E. Reisler and E. M. De La Cruz, *Biophys. J.*, 2011, **101**, 151–159.
20 G. B. Arfken, *Mathematical methods for physicists*, Academic Press, 4th edn, 2013, p. 539.
21 N. W. Ashcroft and N. D. Mermin, *Solid State Physics*, Cengage Learning, 2011.
22 M. Rubinstein and R. H. Colby, *Polymer Physics*, Oxford University Press, 2003.
23 M. Goulian, R. Bruinsma and P. Pincus, *Europhys. Lett.*, 1993, **22**, 145–150.
24 R. Golestanian, M. Goulian and M. Kardar, *Phys. Rev. E: Stat., Nonlinear, Soft Matter Phys.*, 1996, **54**, 6725–6734.
25 M. Kardar and R. Golestanian, *Rev. Mod. Phys.*, 1999, **71**, 1233–1245.
26 E. F. Koslover and A. J. Spakowitz, *Phys. Rev. Lett.*, 2009, **102**, 178102.
27 H. Zhang and J. F. Marko, *Phys. Rev. E: Stat., Nonlinear, Soft Matter Phys.*, 2010, **82**, 051906.
28 W. M. Simpson and U. Leonhardt, *Forces of the quantum vacuum: An Introduction to Casimir Physics*, World Scientific, 2015.
29 H. B. G. Casimir, *Proc. K. Ned. Akad. Wet.*, 1948, 793–795.